J Mol Model (2010) 16:1415–1420
DOI 10.1007/s00894-010-0662-3

ORIGINAL PAPER

Analysis of anisotropic effects in trinuclear metal carbonyl compounds by visualization of through-space NMR shielding

Martha T. de Araujo · Eluzir P. Chacon · José W. de M. Carneiro · Andreas Koch · Erich Kleinpeter

Received: 19 November 2009 / Accepted: 9 January 2010 / Published online: 17 February 2010
© Springer-Verlag 2010

Abstract Through-space NMR shieldings were calculated for trinuclear metal-carbonyl compounds $[M_3(CO)_{12}]$ (M = Fe, Ru, Os), employing the nucleus-independent chemical shift approach. The through-space shieldings were visualized as a contour plot of iso-chemical shielding surfaces, and were applied to quantify the overall anisotropic effect of the carbonyl groups, as well as to identify the influence of the transition metal on the scopes of the corresponding anisotropy cones. The shielding surfaces show that the anisotropic effect of the carbonyl groups at equatorial positions changes depending on the metal. This effect was associated with π–backdonation from the metal to the carbonyl groups in that position, in agreement with geometric data as well as calculated NMR parameters. Therefore, visualization of the through-space NMR shieldings of trinuclear metal-carbonyl compounds of group 8 is able to reflect the distinct arrangements of the carbonyl groups in these organometallic compounds.

Keywords Through-space NMR shielding · Metal-carbonyl compounds · NICS · ICSS · DFT calculations

M. T. de Araujo (✉)
Departamento de Físico-Química,
Universidade Federal Fluminense,
Outeiro de São João Batista, s/n,
24020-150 Niterói, RJ, Brazil
e-mail: mtaraujo@vm.uff.br

E. P. Chacon · J. W. de M. Carneiro
Departamento de Química Inorgânica,
Universidade Federal Fluminense,
Outeiro de São João Batista, s/n,
24020-150 Niterói, RJ, Brazil

A. Koch · E. Kleinpeter
Universität Potsdam, Chemisches Institut,
P.O. Box 60 15 53, 14415 Potsdam, Germany

Introduction

Trinuclear metal-carbonyl compounds of group 8, $[M_3(CO)_{12}]$ (M = Fe, Ru, Os), are important precursors in organometallic chemistry, since they are used as starting materials in the production of a large variety of other organometallic compounds [1–3]. The $[Fe_3(CO)_{12}]$ complex is the most studied species in this group. Its structure has two bridging carbonyl groups and C_{2v} symmetry [4, 5]. The $[Ru_3(CO)_{12}]$ and $[Os_3(CO)_{12}]$ complexes have structures with all of the carbonyl groups at terminal positions in D_3 (quasi D_{3h}) symmetry (Fig. 1) [6–9]. Theoretical calculations [10–13] support the experimental findings.

Recently, the sigma aromaticity model [14, 15] was employed to account for the higher stability of these metal triangles relative to other congener metal polygons [16]. Nucleus-independent chemical shift (NICS) analysis showed quantitative evidence of sigma aromaticity/antiaromaticity in the $[M_3(CO)_{12})]/[M_4(CO)_{16})]$ (M = Fe, Ru, Os) complexes [16]. The NICS technique [17] computes the absolute chemical shielding of a virtual nucleus (ghost atom) at chosen points in the vicinity of the molecule. An NICS value of <0 at the center of a ring indicates the presence of induced diatropic ring currents or aromaticity, whereas an NICS value of >0 indicates induced paratropic ring currents or antiaromaticity. Among the methods based on magnetic properties [18–20], NICS has become the most widely used aromaticity probe due to its simplicity and efficiency [21–24]. This concept can also be employed to visualize the through-space NMR shieldings of molecules via a contour plot of iso-chemical shielding surfaces, whereby the molecule is placed at the center of a grid of ghost atoms, and chemical shieldings are calculated for each point in the grid. It is then possible to gain quantitative information about the spatial extent of the anisotropy effects originating, for

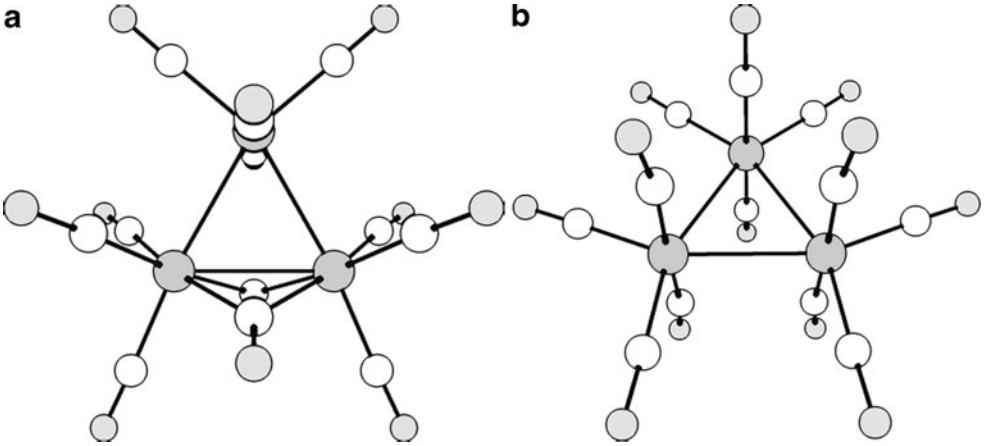

Fig. 1 Structures of $[M_3(CO)_{12}]$ complexes. **a** M = Fe (C_{2v}). **b** M = Ru and Os (D_{3h})

example, from unsaturated chemical bonds [25, 26] and ring currents of aromatic systems [27, 28]. Visualization of the sign and scope of the anisotropy effect gives a clear indication of shielding or deshielding positions.

In the present work we calculated the through-space NMR shielding values for trinuclear metal-carbonyl compounds $[M_3(CO)_{12}]$ (M = Fe, Ru, Os) in order to quantify the overall anisotropic effect of the carbonyl groups, as well as to identify the influence of the transition metal on the scopes of the corresponding anisotropy cones. In particular, we were interested in determining the effects of bridging and terminal (axial and equatorial) carbonyl groups on the relative energies of conformers and their contributions to structural stabilization.

Methodology

$[M_3(CO)_{12}]$ clusters can exist in one of three conformations with $C_{2v,}$ D_3 or D_{3h} symmetry. The $[Fe_3(CO)_{12}]$ complex is found in the C_{2v} symmetry, with two bridging carbonyl groups [4, 5], while $[Ru_3(CO)_{12}]$ and $[Os_3(CO)_{12}]$ are found in the D_3 arrangement, with all carbonyl groups in terminal positions [6–9]. We fully optimized the geometries of each $[M_3(CO)_{12}]$ complex in the three conformations, and confirmed that the doubly bridged arrangement is the ground state for the $[Fe_3(CO)_{12}]$ case and that the all-terminal arrangement is the ground state for the $[Ru_3(CO)_{12}]$ and $[Os_3(CO)_{12}]$ complexes. Calculation of the Hessian matrix confirmed that the C_{2v} geometry is the true minimum for $[Fe_3(CO)_{12}]$ and the D_3 geometry is the minimum for both $[Ru_3(CO)_{12}]$ and $[Os_3(CO)_{12}]$. All geometric optimization and energy calculations were done with the hybrid B3LYP functional [29, 30]. For $[Fe_3(CO)_{12}]$, three different basis sets were employed: 6–31G(d) [31, 32], 6–31+G(d) [33] and LANL2DZ [34, 35]. LANL2DZ is a pseudopotential that includes the D95V basis set for the valence electrons and a relativistic effective potential for the core electrons. Only the LANL2DZ pseudopotential was used for $[Ru_3(CO)_{12}]$ and $[Os_3(CO)_{12}]$.

The same combination of functional and basis sets was used to calculate ^{13}C relative chemical shifts using the gauge-independent atomic orbital (GIAO) approach [36, 37] and tetramethylsilane (TMS) as a reference, calculated at the same level. NICS values, in ppm, were computed using the GIAO method at the same theoretical level as described above. The ghost atoms were placed on a lattice of 10 to −10 Å with a step size of 0.5 Å in the three dimensions. The resulting NICS values were then transformed into a contour file. Shielding surfaces were obtained for values of −5.0, −2.0, −1.0, −0.5 and −0.1 ppm shielding and 0.1 ppm deshielding.

All calculations were done with the Gaussian 03 package [38]. The shielding/deshielding surfaces were visualized using the SYBYL software [39].

Results and discussion

Bridging $[Fe_3(CO)_{12}]$ structure

The C_{2v} structure of the $[Fe_3(CO)_{12}]$ complex calculated with the LANL2DZ pseudopotential is the most stable arrangement. The relative energies found for the D_3 and D_{3h} structures are 1.87 and 12.23 kcal mol^{-1}, respectively, thus confirming experimental findings [40].

The through-space NMR shieldings of $[Fe_3(CO)_{12}]$, calculated at the different theoretical levels, are shown in Fig. 2. This figure clearly indicates that the shielding/deshielding surfaces are quite similar for the three methods. A shielding surface (yellow) is seen along the bond axis of the carbonyl groups. A deshielding surface (red) is found perpendicular to the bond axis of the carbonyl groups. The through-space shieldings are strongly influenced by the anisotropic effects of the carbonyl groups, as indicated by the overlap of the

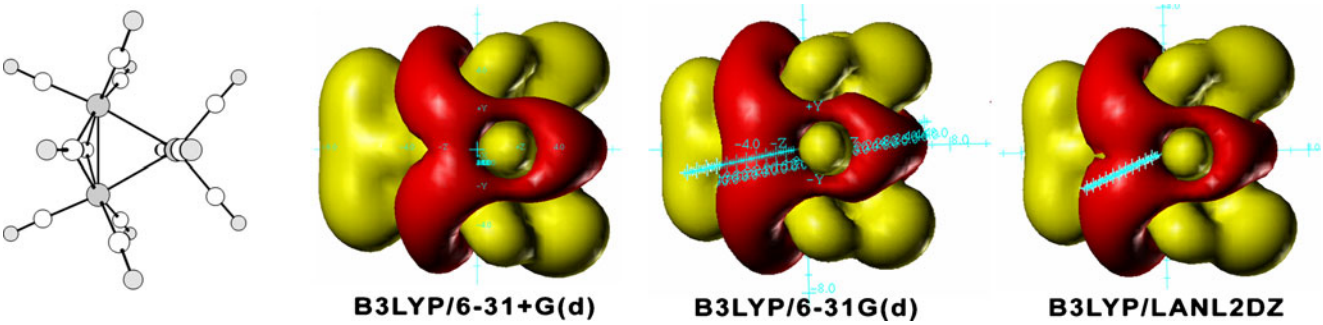

Fig. 2 Shielding surfaces of $[Fe_3(CO)_{12}]$, C_{2v} symmetry, at different theoretical levels, where a *yellow surface* represents −0.1 ppm shielding and a *red surface* represents 0.1 ppm deshielding

corresponding deshielding surfaces (red) of the carbonyl groups with the center of the ring. Table 1 shows the NICS values calculated at the center of the ring along the direction normal to the ring plane (the z-direction). The effects on the chemical shifts of those virtual nuclei are shielding from zero until 2 Å above or below the metal plane, and deshielding beyond this limit.

The ^{13}C NMR spectrum of $[Fe_3(CO)_{12}]$ was calculated to evaluate the degree of shielding/deshielding on the carbonyl carbons. Table 2 shows the ^{13}C chemical shifts calculated at different theoretical levels, as well as those measured by solid-state NMR [41, 42]. The ^{13}C resonances observed for the carbonyl groups, in ppm, from either 25 °C or −93 °C, follow the sequence: bridging (C_4, C_5) > axial (C_{22}, C_{23}) > pseudo-axial (C_{12}, C_{15}) > equatorial (C_{20}–C_{21}) > pseudo-equatorial (C_8, C_9), according to their positions on the triangular ring. For the static structure (T=−93 °C), the difference between the axial (pseudo-axial) and equatorial (pseudo-equatorial) chemical shifts is 18(11) ppm. The theoretical results are in qualitative agreement with the experimental ones, although smaller positive deviations are found using the 6–31G(d) basis set. In this case, the carbon atoms at the equatorial positions are nearly 11 ppm more shielded than those at the axial positions.

Figure 2 shows that the anisotropic effect of the carbonyl groups, which exhibits shielding surfaces (yellow) along the bond axis, is strengthened at the equatorial positions compared to that at the axial positions. This result indicates that there is a correlation between the intensity of the anisotropic effect and the ^{13}C chemical shift. The magnetic shielding is larger at equatorial positions where the carbonyl carbons are more heavily shielded, so they display lower chemical shifts.

Table 1 NICSs (ppm) calculated for $[Fe_3(CO)_{12}]$ along the z-direction passing through the center of the ring

Distance (Å)	B3LYP/ 6-31+G(d)	B3LYP/ 6-31G(d)	B3LYP/ LANL2DZ
2.5	0.36	0.99	0.82
2.0	−0.18	0.00	−0.30
1.5	−7.06	−6.81	−5.67
1.0	−20.34	−18.49	−17.51
0.5	−34.06	−29.97	−29.97
0.0	−41.15	−36.10	−36.37

$[M_3(CO)_{12}]$ structures with all of the carbonyls at terminal positions

As mentioned before, the most stable structure of $[Fe_3(CO)_{12}]$ has two bridging carbonyl groups with C_{2v} symmetry. The

Table 2 Relative isotropic ^{13}C chemical shifts, δ(ppm) from TMS, for $[Fe_3(CO)_{12}]$ calculated at different theoretical levels, and those measured by solid-state NMR

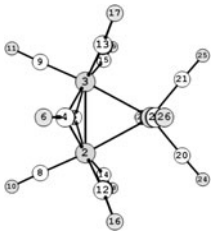

Atom	B3LYP/ 6-31+G(d)	B3LYP/ 6-31G(d)	B3LYP/ LANL2DZ	Exp[a] T=25°C	Exp[b] T=−93°C
C-4	263.14	256.26	284.85	226.1	238.8
C-5	263.14	256.26	284.85	224.5	236.5
C-8	213.88	208.63	236.63	203.2	198.3
C-9	213.88	208.63	236.63	201.8	198.3
C-12	224.28	220.43	249.73	210.2	209.5
C-13	224.28	220.43	249.73	214.1	209.5
C-14	224.28	220.43	249.73	214.1	209.5
C-15	224.28	220.43	249.73	210.2	209.5
C-20	222.17	217.12	246.52	201.8	198.3
C-21	222.17	217.12	246.52	203.2	198.3
C-22	232.48	227.98	257.13	224.5	216.0
C-23	232.48	227.98	257.13	226.1	216.0

[a] [41], [b] [42]

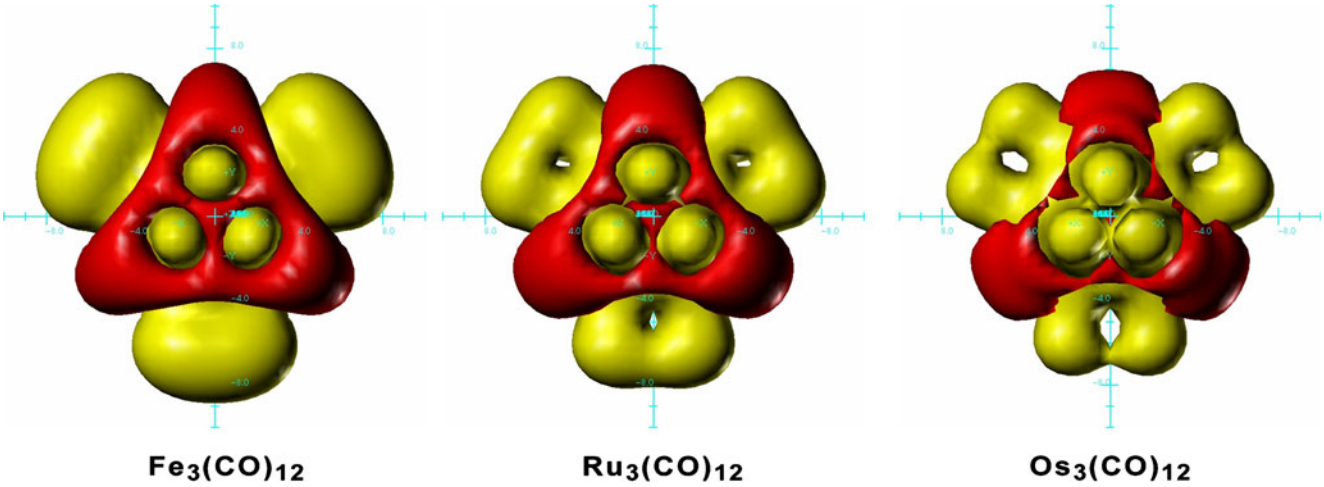

Fig. 3 Shielding surfaces of $M_3(CO)_{12}$, D_{3h} symmetry, where a *yellow surface* represents −0.1 ppm shielding and a *red surface* represents 0.1 ppm deshielding

$[Ru_3(CO)_{12}]$ and $[Os_3(CO)_{12}]$ clusters both have minimum energy structures with D_3 symmetry, although the D_{3h} form is only slightly higher in energy. For the bridged $[Fe_3(CO)_{12}]$ structure, we found that the anisotropic effects of the carbonyl groups in the axial or equatorial positions correlate with the ^{13}C chemical shift. It is thus worth analyzing the same effect in $[Ru_3(CO)_{12}]$ and $[Os_3(CO)_{12}]$. To better differentiate between the two positions (axial and equatorial),

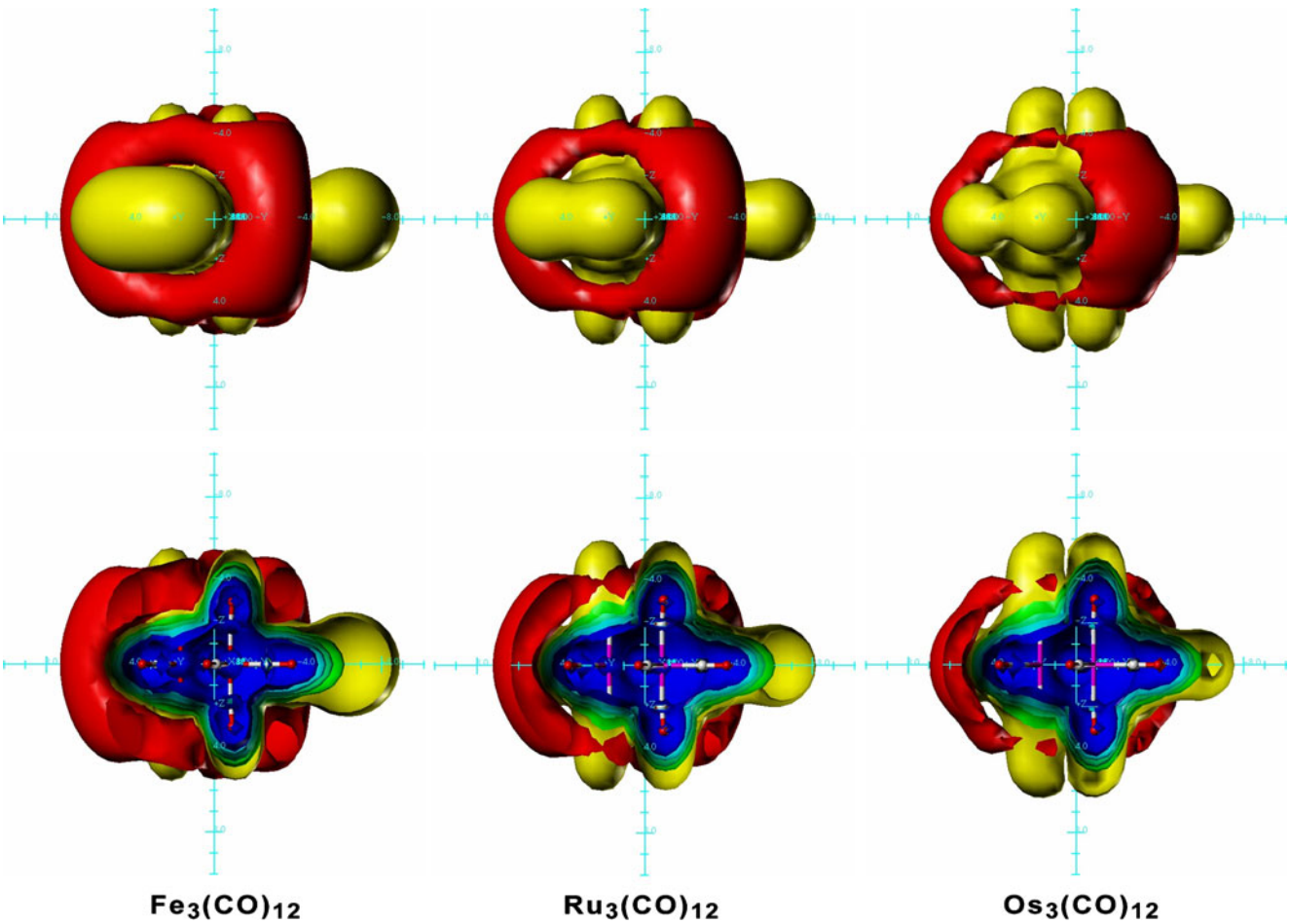

Fig. 4 Shielding surfaces of $[M_3(CO)_{12}]$, D_{3h} symmetry. The *blue*, *cyan*, *blue-green*, *green* and *yellow surfaces* represent, respectively, −5, −2, −1, −0.5 and −0.1 ppm shielding, while a *red surface* represents 0.1 ppm deshielding

we only analyzed the D_{3h} structures. As there is no all-electron basis set for Ru and Os, the B3LYP/LANL2DZ combination was used to calculate the through-space NMR shielding values of the D_{3h} structures. The calculated values for the shielding surfaces of the D_{3h} structures (Fig. 3) confirm that the anisotropic effect of the carbonyl groups is strengthened at equatorial positions compared to the corresponding axial positions. The shielding surface values decrease in the sequence Fe > Ru > Os. Figure 4 shows shielding surfaces at −0.1 ppm (yellow) for the carbonyl groups at the equatorial positions in the Fe, Ru and Os clusters at 9, 8 and 7 Å from the center of the ring, respectively. The distance between the oxygen atom and the green shielding surface at −0.5 ppm (green) also decreases in the same order. In contrast to this, the anisotropic effects of the carbonyl groups at axial positions increase from Fe to Os.

The ^{13}C chemical shifts of the D_{3h} structures (Table 3) were calculated using the 6–31G(d) basis set for oxygen and carbon atoms and the LANL2DZ pseudopotential for the metals. The same behavior as that found for $[Fe_3(CO)_{12}]$ (C_{2v} symmetry) was observed for the D_{3h} structures. The carbonyl carbons at equatorial positions are more shielded than those at axial positions. The differences in chemical shift ($\Delta\delta$) between the axial and equatorial positions for the $[Fe_3(CO)_{12}]$ and $[Ru_3(CO)_{12}]$ clusters are quite similar: 23.04 and 25.71 ppm, respectively. This difference is substantially reduced to 14.66 ppm for $[Os_3(CO)_{12}]$. Considering the synergistic nature of the M–CO bond in these systems, it may be postulated that the increase in the anisotropic effect at equatorial positions may be related to better π–backdonation from the metal to the carbonyl groups, contributing to better electron delocalization and a stronger anisotropic effect. The differences between the axial and equatorial shielding surfaces decrease from Fe to Os. Because of the higher polarizability of the heavier metal, the degree of electron backdonation tends to even out the shielding effects at the two positions for osmium.

An analysis of geometric data (Tables 4 and 5) supports this proposition. The O...O and C...C distances between two equatorial carbonyl groups are bigger than the equivalent distances between axial carbonyls (Table 4). This indicates that the overlap of the yellow shielding surfaces seen at the equatorial positions is not due to the carbonyl groups being in closer proximity, but to a stronger anisotropic effect (see Figs. 2 and 3). The M–C–O angles at the axial positions are more distorted than those at the equatorial ones: Fe (170.87/178.39°), Ru (171.65/178.41°) and Os (174.41/179.08°). This stronger distortion can be attributed to steric electronic hindrance due to the three axial carbonyl groups above and below the plane of the ring. This distortion may decrease the π–backdonation and the electron delocalization at the axial positions. In addition, M–CO bond lengths at equatorial positions are shorter, and the electronic charges on the O atoms are larger at equatorial positions than at axial ones (Table 5), reinforcing our proposal.

Table 3 Isotropic ^{13}C chemical shift, δ(ppm) from TMS, of $[M_3(CO)_{12}]$ calculated with B3LYP/6-31G(d)/LANL2DZ

Metal	C-axial	C-equat.	Δδ
Fe	238.65	215.61	23.04
Ru	229.66	203.95	25.71
Os	213.94	199.28	14.66

Table 4 O…O and C…C distances (Å) between two equatorial carbonyl groups and two axial carbonyl groups, and M–C–O angles at axial and equatorial positions

Metal	C...C axial	C...C equat.	O...O axial	O...O equat.	M–C–O (°) axial/equat.
Fe	2.73	2.83	3.05	3.57	170.87/178.39
Ru	2.87	3.47	3.13	3.86	171.65/178.41
Os	2.92	3.51	3.09	3.89	174.41/179.08

Conclusions

Visualization of the through-space NMR shieldings of trinuclear metal-carbonyl compounds $[M_3(CO)_{12}]$ (M = Fe, Ru, Os) shows that the shielding/deshielding surfaces are quite similar for different calculation levels. The carbonyl groups display shielding (yellow) along the bond axis and deshielding (red) perpendicular to the bond axis. The anisotropic effect of the carbonyl groups is strengthened at equatorial positions. Considering the synergistic nature of the M–CO bonding in these systems, it may be postulated that the increase in the anisotropic effect at equatorial positions may be related to better π–backdonation from the metal to the carbonyl groups, which is associated with better electron delocalization, since at those positions the M–C distances are smaller, the charges on the O atoms are greater, and the M–C–O angles are less distorted, resulting in a stronger anisotropic effect. This effect decreases from Fe to

Table 5 M–C distances (Å) and Mulliken charges on O atoms at axial and equatorial positions

Metal	M–C axial (Å)	M–C equat. (Å)	Charge on axial O	Charge on equat. O
Fe	1.811(1.819)[a]	1.785(1.791)[a]	−0.116	−0.134
Ru	1.959(1.942)[b]	1.933(1.921)[b]	−0.095	−0.101
Os	1.958(1.946)[c]	1.927(1.912)[c]	−0.089	−0.103

[a,b,c] Experimental average values, [a] [40], [b] [8], [c] [9]

Os. Metal clusters with higher polarizabilities show less of a difference in the anisotropic effect between the axial and equatorial positions. Our discussion is supported by solid-state NMR experiments for $[Fe_3(CO)_{12}]$, which show that the ^{13}C chemical shifts at equatorial positions are shifted upfield by 20 ppm compared to those at axial positions. The ^{13}C NMR spectra calculated for these species are qualitatively in agreement with the experimental ones.

Acknowledgments This work was carried out while M.T.A. was at the Universität Potsdam under the auspices of the Deutscher Akademischer Austauschdienst (DAAD)-Coordenação de Aperfeiçoamento de Pessoal de Nível Superior (CAPES) Exchange Program. J.W.M.C. has a research fellowship from Conselho Nacional de Desenvolvimento Científico e Tecnológico (CNPq).

References

1. Dupont J (2005) Química organometálica: elementos do Bloco d. Bookman, Porto Alegre, p 300
2. Crabtree RH (2005) The organomettalic chemistry of transition metals, 4th edn. Wiley, New York
3. Cotton FA, Wilkinson G, Murillo CA, Bochmann M (2005) Advanced inorganic chemistry, 6th edn. Wiley, New York
4. Wei CH, Dahl LF (1969) J Am Chem Soc 91:1351–1361
5. Cotton FA, Troup JM (1974) J Am Chem Soc 96:4155–4159
6. Corey ER, Dahl LF (1961) J Am Chem Soc 83:2203–2204
7. Corey ER, Dahl LF (1962) Inorg Chem 1:521–526
8. Churchill MR, Hollander FJ, Hutchinson JP (1977) Inorg Chem 16:2655–2659
9. Churchill MR, DeBoer BG (1977) Inorg Chem 16:878–884
10. Jang JH, Lee JG, Lee H, Xie Y, Schaefer HF III (1988) J Phys Chem A 102:5298–5304
11. Hunstock E, Mealli C, Calhorda MJ, Reinhold J (1999) Inorg Chem 38:5053–5060
12. Wang H, Xie Y, King RB, Schaefer HF III (2006) J Am Chem Soc 128:11376–11384
13. Chacon EP (2007) Estruturas e Propriedades dos Compostos Carbonílicos Mono e Trinucleares de Metais do Grupo 8 (Ph.D. thesis). Universidade Federal Fluminense, Niterói
14. Dewar MJS, McKee ML (1980) Pure Appl Chem 52:1431–1441
15. Dewar MJS (1984) J Am Chem Soc 106:669–682
16. Corminboeuf C, Schleyer PvR, King RB (2007) Chem Eur J 13:978–984
17. PvR S, Maerker C, Dransfeld A, Jiao H, van Eikema-Hommes NJR (1996) J Am Chem Soc 118:6317–6318
18. Bühl M, Hirsch A (2001) Chem Rev 101:1153–1184
19. Heine T, Corminboeuf C, Seifert G (2005) Chem Rev 105:3889–3910
20. Geuenich D, Hess K, Köller F, Herges R (2005) Chem Rev 105:3758–3772
21. Chen Z, Wannere CS, Corminboeuf C, Puchts R, Schleyer PvR (2005) Chem Rev 105:3842–3888
22. Tsipis AC, Kedalidis CE, Tsipis CA (2007) J Am Chem Soc 129:13905–13922
23. Muñiz J, Sansores LE, Martinez A, Salcedo R (2008) J Mol Model 6:67–75
24. Martin NH, Caldwell BW, Carlson KP, Teague MR (2009) J Mol Graph Mod 27:689–692
25. Klod S, Kleinpeter E (2001) J Chem Soc Perkin Trans 2:1893–1898
26. Klod S, Kleinpeter E (2004) J Am Chem Soc 126:2231–2236
27. Kleinpeter E, Klod S, Koch A (2007) J Mol Struct 811:45–60
28. Kleinpeter E, Klod S, Koch A (2007) J Org Chem 73:1498–1507
29. Becke AD (1993) J Chem Phys 98:5648–5652
30. Lee CT, Yang WT, Parr RG (1988) Phys Rev B 37:785–789
31. Ditchfield R, Hehre WR, Pople JAJ (1971) Chem Phys 54:724–728
32. Hehre WR, Ditchfield R, Pople JAJ (1972) Chem Phys 56:2257–2261
33. Clark T, Chandrasekhar J, Spitznagel GW, Schleyer PvR (1983) J Comput Chem 4:294–301
34. Hay PJ, Wadt WRJ (1985) Chem Phys 82:270–283
35. Hay PJ, Wadt WRJ (1985) Chem Phys 82:299–310
36. Ditchfield JR (1974) Mol Phys 27:789–807
37. Cheeseman JP, Trucks GW, Keith TA, Frisch MJ (1996) J Chem Phys 104:5497–5509
38. Frisch MJ, Trucks GW, Schlegel HB, Scuseria GE, Robb MA, Cheeseman JR, Montgomery JA, Vreven T Jr, Kudin KN, Burant JC, Millam JM, Iyengar SS, Tomasi J, Barone V, Mennucci B, Cossi M, Scalmani G, Rega N, Petersson GA, Nakatsuji H, Hada M, Ehara M, Toyota K, Fukuda R, Hasegawa J, Ishida M, Nakajima T, Honda Y, Kitao O, Nakai H, Klene M, Li X, Knox JE, Hratchian HP, Cross JB, Adamo C, Jaramillo J, Gomperts R, Stratmann RE, Yazyev O, Austin AJ, Cammi R, Pomelli C, Ochterski JW, Ayala PY, Morokuma K, Voth GA, Salvador P, Dannenberg JJ, Zakrzewski VG, Dapprich S, Daniels AD, Strain MC, Farkas O, Malick DK, Rabuck AD, Raghavachari K, Foresman JB, Ortiz JV, Cui Q, Baboul AG, Clifford S, Cioslowski J, Stefanov BB, Liu G, Liashenko A, Piskorz P, Komaromi I, Martin RL, Fox DJ, Keith T, Al-Laham MA, Peng CY, Nanayakkara A, Challacombe M, Gill PMW, Johnson B, Chen W, Wong MW, Gonzalez C, Pople JA (2003) Gaussian 03, revision A.1. Gaussian Inc., Pittsburgh
39. Tripos (2005) Sybyl 7.1. Tripos, St. Louis
40. Braga D, Farrugia LJ, Grepioni F, Johnson BFG (1994) J Organomet Chem 464:C39–C41
41. Dorn H, Hanson BE, Motell E (1981) Inorg Chem Acta 54:L71–L73
42. Hanson BE, Lisic EC, Petty JT, Iannaconne GA (1986) Inorg Chem 25:4062–4064